2008

# Flicker Attenuation—Part II: Transfer Coefficients for Regular Voltage Fluctuations in Radial Power Systems With Induction Motor Loads

S. Tennakoon
*University of Wollongong*

S. Perera
*University of Wollongong*, sarath@uow.edu.au

D. Robinson
*Beca Pty Ltd, Australia*

# Flicker Attenuation—Part II: Transfer Coefficients for Regular Voltage Fluctuations in Radial Power Systems With Induction Motor Loads


## Abstract

Electromagnetic compatibility standards and guidelines used for planning of flicker allocation at various busbars of a power system requires some knowledge of the manner in which voltage fluctuations and hence the flicker propagate and how various loads respond to them. The current rudimentary approach taken for the determination of the load response to voltage fluctuations is based on network impedance values and hypothetical dynamic impedance values of the connected loads. Practical results and recently developed theory on the subsynchronous behavior of induction machines suggest that where there is a large base of induction machine exists on a power system the flicker attenuation is significant. This paper reports on a methodology to include the influence of induction machine behavior in flicker propagation and attenuation studies. The work is based on small-signal models to describe induction machine and system behavior which are utilized for the development of a flicker transfer coefficient. A systematic approach for the practical application of the methodology for flicker related work is included.



## Keywords

Flicker, flicker attenuation, induction motors, voltage fluctuations.


## Disciplines

Physical Sciences and Mathematics


## Publication Details

This article was originally published Tennakoon, S, Perera, S & Robinson, D, Flicker Attenuation—Part II: Transfer Coefficients for Regular Voltage Fluctuations in Radial Power Systems With Induction Motor Loads, IEEE Transactions on Power Delivery, 23(2), 2008, 1215-1221.

# Flicker Attenuation—Part II: Transfer Coefficients for Regular Voltage Fluctuations in Radial Power Systems With Induction Motor Loads

S. Tennakoon, *Student Member, IEEE*, S. Perera, *Member, IEEE*, and D. Robinson

***Abstract*—Electromagnetic compatibility standards and guidelines used for planning of flicker allocation at various busbars of a power system requires some knowledge of the manner in which voltage fluctuations and hence the flicker propagate and how various loads respond to them. The current rudimentary approach taken for the determination of the load response to voltage fluctuations is based on network impedance values and hypothetical dynamic impedance values of the connected loads. Practical results and recently developed theory on the subsynchronous behavior of induction machines suggest that where there is a large base of induction machine exists on a power system the flicker attenuation is significant. This paper reports on a methodology to include the influence of induction machine behavior in flicker propagation and attenuation studies. The work is based on small-signal models to describe induction machine and system behavior which are utilized for the development of a flicker transfer coefficient. A systematic approach for the practical application of the methodology for flicker related work is included.**

***Index Terms*—Flicker, flicker attenuation, induction motors, voltage fluctuations.**

## I. Introduction

VOLTAGE fluctuations leading to lamp flicker caused by loads such as electric arc furnaces can penetrate into the power system by propagating though the transmission, subtransmission, and distribution systems. Flicker propagation through different voltage levels takes place with some level of attenuation depending on several factors including system impedance, frequency components that are present in the fluctuating voltage waveform and load composition [1]–[4]. Synchronised measurement campaigns [5] and other measurement programmes support the concept of flicker attenuation and suggest that large proportions of inductions motors assist in attenuating flicker compared to residential loads consisting of passive devices. In existing methods of flicker transfer analysis, induction motors are usually represented by a hypothetical dynamic impedance which is assumed to be the transient impedance of conventional third order induction motor model used for other dynamic system studies. This representation would be insufficient for flicker studies as voltage fluctuations responsible for flicker contain numerous frequency components, whereas the traditional dynamic induction motor models reflect the motor response to voltage changes of fundamental frequency only. Hence, flicker transfer and attenuation studies involving induction motors require further detailed modelling of systems containing induction motors.

Response of inductions motors of different ratings to two types of regular voltage fluctuation conditions are covered in [6]. The work presented in this paper is an extension to what is presented in [6]. The main objective is to develop a suitable theoretical basis to investigate contribution of induction motor loads towards attenuating flicker in radial power systems, using the induction motor response established in [6].

This paper is organized as follows. Section II gives a brief overview highlighting the manner in which flicker transfer becomes applicable in relation to flicker allocation in power systems based on the IEC, AS/NZS standards. The extension of the small-signal induction motor model which has been used in [6] is discussed in Section III. The analysis of upstream to downstream flicker transfer in a radial power system having a downstream induction motor load is presented in Section IV. The determination of flicker transfer coefficient using the small-signal model, and evaluation of the accuracy of small-signal modelling, are discussed in Section V. Conclusions are given in Section VI

## II. Brief Overview of the Approach Based on IEC 61000-3-7, AS/NZS61000.3.7 for Flicker Allocation

Estimation of the propagation of flicker from one bus to another bus for the purpose of allocating flicker emission as per IEC, AS/NZS standards [7], [8] relies on the flicker transfer coefficient and influence coefficient. The use of transfer coefficient is demonstrated through the use of the short-term flicker transfer coefficient from high voltage (HV) to medium voltage (MV), $T_{PstHM}$, in (1) to determine the global short-term flicker emission limit ($G_{stMV}$) for all loads supplied at MV

$$G_{PstMV} = \sqrt[3]{L_{PstMV}^3 - T_{PstHM}^3 L_{PstHV}^3} \qquad (1)$$

where $L_{PstMV}$ is the MV flicker planning level and $L_{PstHV}$ is the HV flicker planning level.

According to (1), a conservative value of unity flicker transfer coefficient (i.e., $T_{PstHM} = 1$) will overestimate the flicker levels transferred from HV to MV level causing unnecessary limitations on downstream MV loads. Conversely, a transfer coefficient less than unity can be expected if the downstream consists a significant proportion induction motor loads. Therefore,

Manuscript received January 5, 2007; revised June 14, 2007. This work was supported by TransGrid. Paper no. TPWRD-00829-2006.

S. Tennakoon and S. Perera are with the School of Electrical, Computer and Telecommunications Engineering, University of Wollongong, Wollongong NSW 2522, Austraila and the Integral Energy Power Quality and Reliability Centre, Wollongong NSW 2522, Australia (e-mail: sarath@uow.edu.au).

D. Robinson is with Beca Pty Ltd., Wollongong NSW 2500, Australia.

Digital Object Identifier 10.1109/TPWRD.2008.915826

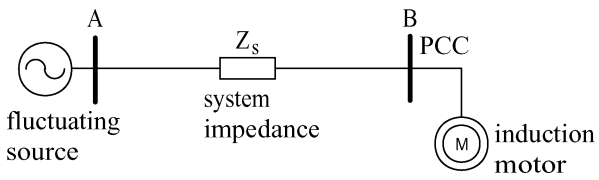


Fig. 1. Radial system.

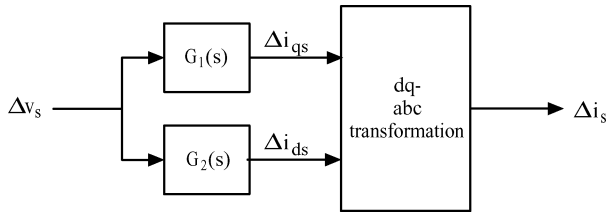


Fig. 2. Block diagram of the small-signal model.

a precise knowledge of $T_{PstHM}$ is essential in determining the total headroom available for the connection of fluctuating loads at downstream MV level.

In interconnected HV systems, the flicker contributions from neighbouring busbars, eg. busbars $B$ and $C$ on another busbar $A$, are taken into account by the use of influence coefficients $K_{B-A}$ and $K_{C-A}$ in (2) for the calculation of the total available power $S_{tHVA}$ at $A$ for allocating the fluctuating load at $A$ $(S_{tHV})$

$$S_{tHV} = S_{tHVA} + K_{B-A}S_{tHVB} + K_{C-A}S_{tHVC} + \dots \quad (2)$$

where $S_{tHVB}$ and $S_{tHVC}$ are the available power levels at busbars $B$ and $C$, respectively.

As in the case of the radial system, the influence coefficients $K_{B-A}$ and $K_{C-A}$ will depend on the nature of the loads connected at the various busbars.

## III. Small-Signal Modelling for Flicker Transfer Analysis

### A. Introduction to the Study System

The system under consideration is a simple radial network as shown in Fig. 1 which consists of a fluctuating voltage supply at upstream (A) and an induction motor load connected to the downstream (B). $Z_s$ represents the system impedance that connects the upstream and the downstream such as transformer impedance. In [6], the response of induction motors to two types of regular voltage fluctuations in the supply, namely: a) the case where a single frequency component (positive or negative sequence) is superimposed on the mains frequency and b) sinusoidal amplitude modulation of the mains frequency has been investigated. In the present work only the type b) voltage fluctuations are considered as it is a classical case considered in flicker related work. However, the proposed methodology allows the use of other types of voltage fluctuations such as square wave or irregular variations.

In order to verify the results obtained using the small-signal modelling presented in this section, studies were also carried out using an induction motor model developed in Matlab/Simulink using well known d-q axes voltage/flux linkage and torque equations. This model has been used in [6] to verify the induction motor response to fluctuations in the supply voltage established employing the small-signal model as well.

A range of induction motors of which parameters are given in [6] and [9] has been examined in the present work as in [6]. The mechanical load driven by each motor is assumed to be of the pump type as described in [6].

### B. Modification to the Small-Signal Model of an Induction Motor to Accommodate the Radial Network

The small-signal model of an induction machine presented in [6] is used to investigate the response of the motor to voltage fluctuations caused by sinusoidal amplitude modulation. This model involves formulation of two fifth order transfer functions ($G_1(s)$ and $G_2(s)$) of which the detailed descriptions are given in [6] and can be represented as per (3) and (4) where, $\Delta v_s$ is a small variation in the amplitude of the supply voltage, $\Delta i_{qs}$ and $\Delta i_{ds}$ are the resultant variations in d-q axes stator currents. Outputs of (3) and (4) have to be transformed to a-b-c (phase) domain in order to reconstruct the resultant change in phase domain stator current $(\Delta i_s)$ as illustrated by Fig. 2

$$G_1(s) = \frac{\Delta i_{qs}}{\Delta v_s} \quad (3)$$

$$G_2(s) = \frac{\Delta i_{ds}}{\Delta v_s.} \quad (4)$$

The above approach can be extended to a radial system shown in Fig. 1 by incorporating the system impedance, $Z_s$ $(Z_s = R_s + jX_s)$ into the stator resistance $(r_s)$ and stator leakage reactance $(X_{ls})$ of the induction motor as per (5)

$$r_{s-new} + jX_{ls-new} = [r_{s-old} + R_s] + j[X_{ls-old} + X_s]. \quad (5)$$

With this modification, outputs of $G_1(s)$ and $G_2(s)$ of Fig. 2 are the changes in the d-q axes stator currents caused by a small change in the amplitude of the upstream (A) voltage when the induction motor is connected to the downstream (B). The established stator current response can be used to determine the instantaneous change in the voltage at B as

$$\Delta v_B(t) = \Delta v_A(t) - L_s \frac{d}{dt}\Delta i_s(t) - R_s \Delta i_s(t) \quad (6)$$

where $\Delta v_A(t)$ and $\Delta v_B(t)$ are the instantaneous voltage changes at A and B, respectively, $L_s = X_s/2\pi f_b$, $f_b$ being the mains or the base frequency.

Based on work presented in [6], a sinusoidal signal is used as $\Delta v_s$ in order to represent a typical sinusoidal amplitude-modulating signal of frequency $f_m$. The frequency of $\Delta v_s$ is varied between 0.01 Hz and 40 Hz covering the perceptible flicker frequency range. The magnitude of $\Delta v_s$ was maintained at 0.05 p.u. which corresponds to a constant magnitude in voltage fluctuation $(\Delta v)$ of 0.1 p.u. $(\Delta v = 2 \times \Delta v_s)$. $\Delta v_s$ will give rise to two voltage side bands (pertubations) at two distinct frequencies at A $(\Delta v_A(t))$ and B $(\Delta v_B(t))$ as

$$\Delta v_A(t) = \Delta v_{ALSB}(t) + \Delta v_{AUSB}(t) \quad (7)$$

$$\Delta v_B(t) = \Delta v_{BLSB}(t) + \Delta v_{BUSB}(t) \quad (8)$$

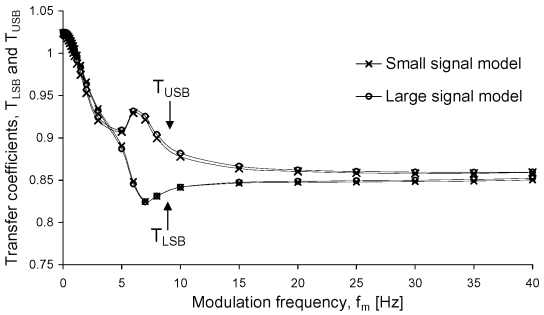


Fig. 3. Variation of transfer coefficients of voltage side bands ($T_{LSB}$ and $T_{USB}$) with modulation frequency ($f_m$) for the 2250 hp machine.

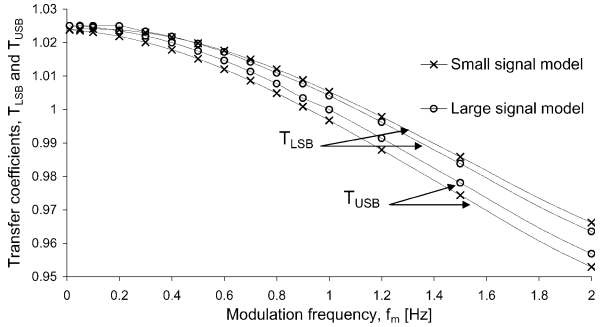


Fig. 4. Variation of transfer coefficients of voltage side bands ($T_{LSB}$ and $T_{USB}$) at low modulation frequencies for the 2250 hp machine.

where $\Delta v_{ALSB}(t)$ and $\Delta v_{BLSB}(t)$ are the lower side band at frequency $f_b - f_m$, $\Delta v_{AUSB}(t)$ and $\Delta v_{BUSB}(t)$ are the upper side band at frequency $f_b + f_m$. Accordingly, two transfer coefficients can be defined for the two voltage side bands as

$$T_{LSB} = \frac{\frac{|\Delta v_{BLSB}|}{|v_B|}}{\frac{|\Delta v_{ALSB}|}{|v_A|}} \tag{9}$$

$$T_{USB} = \frac{\frac{|\Delta v_{BUSB}|}{|v_B|}}{\frac{|\Delta v_{AUSB}|}{|v_A|}} \tag{10}$$

where $v_A$ and $v_B$ are the steady state voltages at A and B, respectively, obtained from a load-flow study.

## IV. Flicker Transfer Analysis Using Small- and Large-Signal Models

### A. Transfer Coefficients for a Radial Power System Having a 2250 hp Induction Machine at Downstream

For a radial network having a purely inductive system impedance ($Z_s = jX_s$) of 3% (of $Z_{FL}$, the base impedance of the motor at full load slip), the side band transfer coefficients ($T_{LSB}$ and $T_{USB}$) are established in relation to a 2250 hp induction motor connected at the downstream busbar (B). Fig. 3 illustrates the variation of $T_{LSB}$ and $T_{USB}$ with the modulation frequency ($f_m$) established using both small-signal and large-signal models over the range of modulation frequencies stated earlier, where good agreement can be noted.

Over a wide range of modulation frequencies, the lower and upper side bands exhibit different attenuation levels where lower side band is seen to attenuate to a better extent compared to the upper side band for modulation frequencies above 5 Hz. A close examination of Fig. 3 at low $f_m$ ($\leq$1 Hz) values reveals that the side bands do not attenuate but rather they get magnified, as illustrated by Fig. 4.

Noting that the two side bands are caused by a single modulation frequency ($f_m$), the transfer coefficient of each voltage side band can be plotted against the frequency of the side band ($f_b \pm f_m$), as illustrated in Fig. 5. As the maximum value of $f_m$ used is 40 Hz, transfer coefficients can be established for side band frequencies in the range 20 Hz ($= 60\ \text{Hz} - 40\ \text{Hz}$) and 100 Hz ($= 60\ \text{Hz} + 40\ \text{Hz}$).

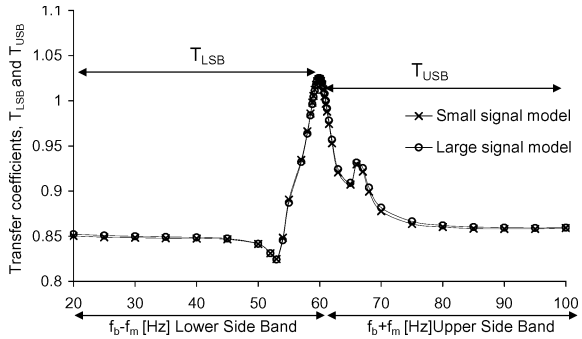


Fig. 5. Variation of transfer coefficients of voltage side bands ($T_{LSB}$ and $T_{USB}$) with side band frequency ($f_b \pm f_m$) for the 2250 hp machine.

### B. Effective Sub or Supersynchronous Impedances, Active and Reactive Power Variations of the 2250 hp Induction Machine

For the purpose of giving a qualitative explanation on the attenuation levels exhibited by the side bands as depicted in Fig. 5, this section establishes the variation of the effective impedances and the corresponding real and reactive power flows with the side band frequency.

Considering the network of Fig. 1 the transfer coefficient $T$ in relation to voltage fluctuations can be expressed as [1]:

$$T = \frac{\frac{|\Delta v_B|}{|v_B|}}{\frac{|\Delta v_A|}{|v_A|}} = \frac{\left|1 + \frac{Z_s}{Z_{\text{motor}}}\right|}{\left|1 + \frac{Z_s}{Z'_{\text{motor}}}\right|} \tag{11}$$

where $\Delta v_A$ and $\Delta v_B$ are the voltage perturbations at A and B, respectively, $Z_{\text{motor}}$ is the steady-state impedance of the motor and $Z'_{\text{motor}}$ is the effective impedance offered by the motor to the voltage perturbation. In (11), for the case of sinusoidal amplitude modulation, $Z'_{\text{motor}}$ could be considered as an effective subsynchronous impedance for the lower side band and an effective supersynchronous impedance for the upper side band. Further, the magnitude and the angle ($\psi$) of the effective impedance of the motor are key factors that determine the extent to which each side band is attenuated at B compared to that present at A, as $Z_s$ represents a static component.

Based on (11) it can be noted that if $Z'_{\text{motor}}$ is inductive ($0° < \psi < 90°$ or $90° < \psi < 180°$), smaller the magnitude of $Z'_{\text{motor}}$ better would be the attenuation of the corresponding voltage side band at B. However, if $Z'_{\text{motor}}$ becomes capacitive ($-90° < \psi < 0°$ or $-180° < \psi < -90°$), regardless of the magnitude of $Z'_{\text{motor}}$, the voltage side band will be magnified at B. Hence

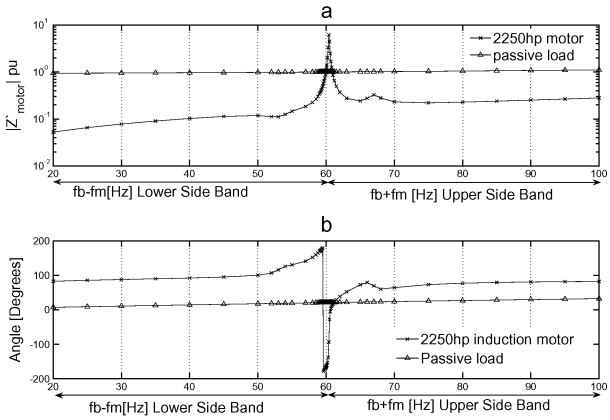


Fig. 6. Variation of (a) the magnitude and (b) angle of the effective impedance of the 2250 hp motor and an equivalent passive load with frequency of the voltage side band $(f_b \pm f_m)$.

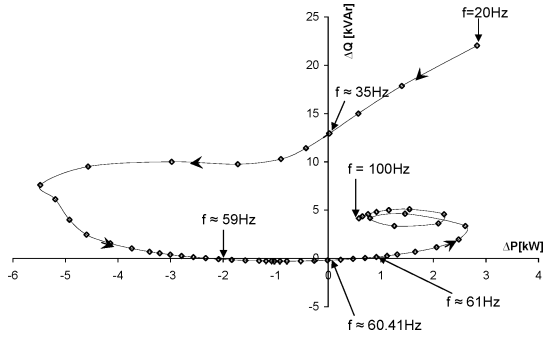


Fig. 7. Active $(\Delta P)$ and reactive $(\Delta Q)$ power consumed by the 2250 hp motor for voltage side bands at $f$, $f = f_b \pm f_m$.

the nature of variation of $Z'_{\rm motor}$ which can be determined using the small-signal analysis has to be examined.

The stator current response of the 2250 hp motor operating with an amplitude modulated supply [6] can be used to determine its effective impedance $(Z'_{\rm motor})$ for each side band as

$$Z'_{\rm motor} = \frac{|\Delta v_B|}{|\Delta i|}\angle\alpha_1 - \alpha_2 = |Z'_{\rm motor}|\angle\psi \qquad (12)$$

where $\Delta i$ is the stator current perturbation ($\Delta i_{LSB}$ or $\Delta i_{USB}$), $\alpha_1$ and $\alpha_2$ are the phase angles of $\Delta v_B$ and $\Delta i$ respectively. Figs. 6(a) and (b) illustrate the variation of $|Z'_{motor}|$ and $\psi$ as a function of the frequency of voltage side bands $(f_b \pm f_m)$. For the purpose of comparison, it can be noted that over the frequency range of interest the magnitude of the impedance and its phase angle of a passive load that is equivalent to the 2250 hp induction motor will be nearly constant in comparison to the variations exhibited by the induction motor.

At the side band frequencies the corresponding active and reactive power of the motor calculated as per (13) are illustrated in the $\Delta P - \Delta Q$ plane of Fig. 7

$$\Delta P + j\Delta Q = \Delta v_B \times \Delta i^*. \qquad (13)$$

### C. Discussion on Attenuation Levels Exhibited by the 2250 hp Machine

*1) Lower Side Band ( LSB);* $20\ \text{Hz} \le f < 60\ \text{Hz}$*:* Based on Fig. 6, for voltage side bands at frequencies between 20 Hz and 59 Hz, magnitude of the effective impedance of the motor is smaller than 1 p.u.. The angle $\psi$ varies between 83° and 90° for $20\ \text{Hz} \le f \le 35\ \text{Hz}$. The same varies between 90° and 180° for $35\ \text{Hz} \le f \le 59\ \text{Hz}$ and implies a negative resistance and an inductive reactance. This behavior is further supported $\Delta P$ and $\Delta Q$ variations illustrated by the Fig. 7.

Over the side band frequency range $20\ \text{Hz} \le f \le 59\ \text{Hz}$, although the machine exhibits both positive and negative damping, it offers an inductive reactance as a part of the effective impedance that is less than unity in magnitude and hence the side bands will attenuate at B. This behavior is illustrated by the $T_{LSB}$ curves in Fig. 3, where the modulation frequency $f_m$ is greater than approximately 1 Hz and in Fig. 5 where frequency of the voltage perturbation $f$ is between 20 and 59 Hz.

For voltage side bands at frequencies just below the fundamental frequency (i.e., $59\ \text{Hz} \le f < 60\ \text{Hz}$), $|Z'_{\rm motor}|$ is less than <1 p.u., yet the angle of $Z'_{\rm motor}$ is negative $(-180° < \phi < -90°)$ exhibiting a negative resistance and a capacitive reactance a behavior that is supported by Fig. 7 where both $\Delta P$ and $\Delta Q$ are negative. Regardless of the relatively small magnitude of $Z'_{\rm motor}$, the capacitive reactance or the over excited nature of the machine would lead to magnification of the corresponding frequency components at downstream (B) for $59\ \text{Hz} \le f < 60\ \text{Hz}$. This behavior is illustrated by $T_{LSB}$ curves in Figs. 4.

*2) Upper Side Band ( USB);* $60\ \text{Hz} < f \le 100\ \text{Hz}$*:* For voltage side bands at frequencies just above the fundamental frequency $(60\ \text{Hz} < f \le 61\ \text{Hz})$, $|Z'_{\rm motor}|$ is relatively large compared to the steady-state impedance and its angle $\psi$ varies between $-90°$ and 0°. This is further evident from Fig. 7, where $\Delta P$ is positive and and $\Delta Q$ is negative. Relatively large magnitude of $|Z'_{\rm motor}|$ and the over-excited behavior causes the magnification of the corresponding frequency components at B.

As is evident from Fig. 6 in the frequency range $61\ \text{Hz} \le f \le 100\ \text{Hz}$, $|Z'_{\rm motor}|$ varies between 0.2 p.u. and 0.3 p.u. and and $\psi$ varies between 0° and 82° indicating its inductive behavior. This is further supported by positive $\Delta P$ and positive $\Delta Q$ in Fig. 7. The positive damping provided by the machine leads to attenuation of the corresponding frequency components as illustrated by $T_{USB}$ curves in Fig. 3.

*3) Difference Between $T_{USB}$ and $T_{LSB}$ in the Modulation Frequency $(f_m)$ Range 5–10 Hz:* According to Fig. 3, $T_{LSB}$ and $T_{USB}$ exhibit values less than unity for most of the modulation frequencies resulting from the relatively small magnitudes of $Z'_{\rm motor}$ as illustrated in Fig. 6 (given using a logarithmic scale). However, a local minimum and a maximum can be seen in $Z'_{\rm motor}$ over the two frequency ranges 50–55 Hz and 65–70 Hz, respectively, leading to a local minimum and a maximum in the voltage transfer coefficient. This effect is reflected on the transfer coefficients $T_{LSB}$ and $T_{USB}$ where a significant difference over the modulation frequency range 5–10 Hz is seen.

### D. Dependency of Transfer Coefficient on the Induction Machine Size

Transfer coefficients of the voltage side bands evaluated for 3 hp and 500 hp machines [6] are illustrated in Fig. 8 along with those of the 2250 hp machine. As in the study in relation to the 2250 hp machine, a totally inductive system impedance $(Z_s)$ of 3% (of $Z_{FL}$, the base impedance of the motor at full load slip)

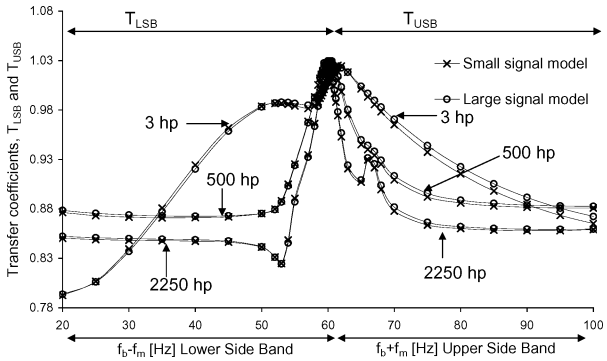


Fig. 8. Variation of transfer coefficients of voltage side bands ($T_{LSB}$ and $T_{USB}$) with side band frequency ($f_b \pm f_m$) for the three machines.

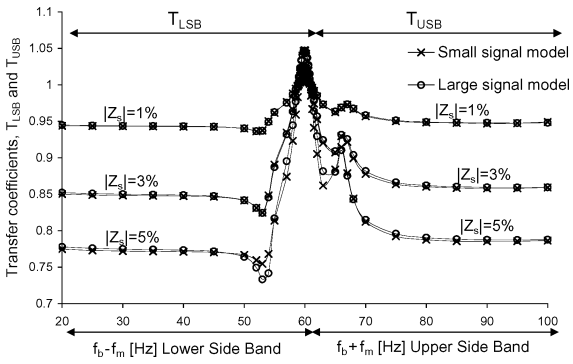


Fig. 9. Variation of transfer coefficients of voltage side bands ($T_{LSB}$ and $T_{USB}$) with side band frequency ($f_b \pm f_m$) for three system impedance ($Z_s = jX_s$) magnitudes—2250 hp machine.

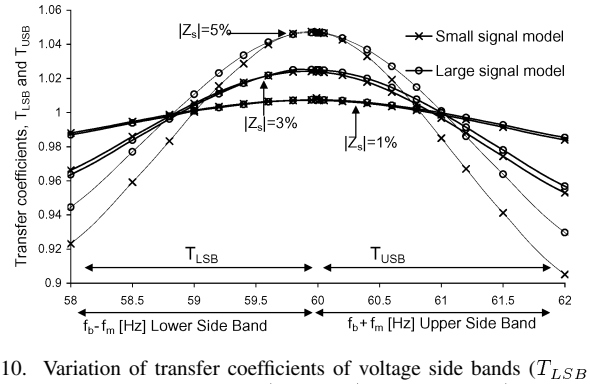


Fig. 10. Variation of transfer coefficients of voltage side bands ($T_{LSB}$ and $T_{USB}$) with side band frequency ($f_b \pm f_m$) for three line ($Z_s = jX_s$) impedance magnitudes at for low modulation frequencies values—2250 hp machine.

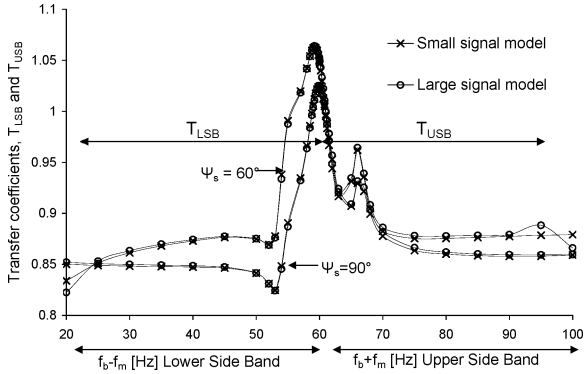


Fig. 11. Variation of transfer coefficients of voltage side bands ($T_{LSB}$ and $T_{USB}$) with side band frequency ($f_b \pm f_m$) for $\psi_s = 90°$ and $\psi_s = 60°$ for the 2250 hp machine.

is used. It is seen that 500 and 2250 hp machines exhibit similar attenuation characteristics. However, the 2250 hp machine attenuates both side bands to a better extent compared to the 500 hp machine. The 3 hp machine is seen to demonstrate somewhat different variations in the side band attenuation levels.

### *E. Dependency of Transfer Coefficient on System Impedance*

The system impedance $Z_s$ was so far assumed to be purely inductive and its magnitude was assumed to be 3% of the impedance of the 2250 hp motor at full load slip. In this section, the influence of the magnitude of system impedance and its angle on side band attenuation is investigated.

*1) Dependency of Transfer Coefficients of Side Bands on the Magnitude of the Inductive System Impedance ($|Z_s|$):* Fig. 9 shows the variation of the transfer coefficients of the voltage side bands with frequency of the side bands for the 2250 hp machine for three different values of the system impedance. As the magnitude of the system impedance is increased, attenuation levels can be seen to increase over a wide range of the side band frequencies. This behavior can be justified using (11). Fig. 10 illustrates the variation of $T_{LSB}$ and $T_{USB}$ for modulation frequencies in the vicinity of the fundamental frequency. As previously discussed side bands tend to magnify at these low frequencies but the level of magnification is seen to decrease for smaller system impedances magnitudes as expected.

*2) Dependency of the Transfer Coefficient of the Side Bands on System Impedance Angle ($\psi_s$):* In the previous results presented, the system impedance was assumed to be purely inductive. The influence of the system impedance angle on flicker attenuation is critical to supply systems with high $X/R$ ratios. In the results presented in this section, system impedance is assumed to be of form $R + jX$.

Fig. 11 illustrates the variation of the transfer coefficients of the side bands for the 2250 hp machine for $\psi_s = 90°$ and $\psi_s = 60°$ while maintaining the magnitude of $Z_s$ constant. It seems reasonable to assume that the attenuation levels depend on the impedance angle where increasingly inductive system impedances favor better attenuation.

## V. Correlation Between the Attenuation of Side Bands and Flicker Attenuation

### *A. Determination of Flicker Transfer Coefficient Using the Small-Signal Model*

The manner in which the voltage side bands of a sinusoidally modulated voltage propagate from upstream to the downstream has been explored in the previous sections. However, these studies cannot be expected to provide a complete insight into flicker transfer as the latter is characterized on the fluctuations in voltage envelope rather than on individual voltage side bands. This section compares side band attenuation levels with the

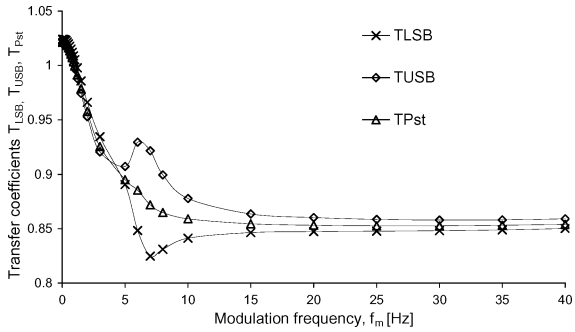


Fig. 12. Comparison of the transfer coefficients of the side bands ($T_{LSB}$ and $T_{USB}$) and flicker transfer coefficient, $T_{Pst}$ for the 2250 hp machine.

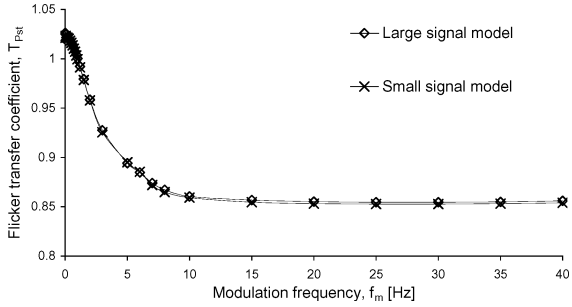


Fig. 13. Comparison of flicker transfer coefficients ($T_{PstAB}$) established using small and large-signal models for the 2250 hp machine.

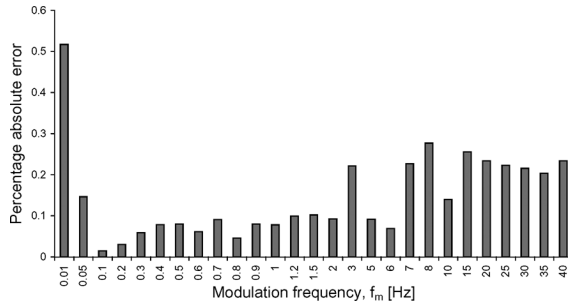


Fig. 14. Percentage error involved in determining flicker transfer coefficient using the small-signal model.

actual flicker present at A and B in the network of Fig. 1. For this purpose, the flicker transfer coefficient is defined ($T_{PstAB}$) as

$$T_{PstAB} = \frac{P_{stB}}{P_{stA}} \tag{14}$$

where $P_{st}$ is the short-term flicker severity and subscripts at A and B denote the corresponding values at A and B respectively. Noting that for regular voltage fluctuations $P_{st}^2 \propto P_{it}$, where $P_{it}$ is the instantaneous flicker sensation, (14) can be re-written as

$$T_{PstAB} = \sqrt{\frac{P_{itB}}{P_{itA}}}. \tag{15}$$

Determination of $P_{itA}$ and $P_{itB}$ requires voltage waveforms at A and B which can be established using the outputs of the small-signal model and the corresponding steady-state voltages. A PC-based flickermeter that has been simulated in PSCAD EMTDC is used to establish $P_{itA}$ and $P_{itB}$. Fig. 12 illustrates the variation of the flicker transfer coefficient ($T_{PstAB}$) and the transfer coefficients of the side bands of the 2250 hp machine with modulation frequency $f_m$.

Fig. 12 indicates that the flicker transfer coefficient is less than unity for most of the modulation frequencies. As $f_m$ increases $T_{PstAB}$ decreases, a behavior that was noted in relation to the side band attenuation as well. Moreover, it is seen that for a given modulation frequency $f_m$, the magnitude of the flicker transfer coefficient lies between the two transfer coefficients of the lower and upper side bands respectively. Contrary to the peak and trough exhibited by the two side bands in relation to attenuation between $f_m = 5$ Hz and $f_m = 10$ Hz, the flicker transfer coefficient does not exhibit a significant shift from its gradual decrease with $f_m$. Fig. 12 also illustrates the flicker magnification at low modulation frequencies similar to what was exhibited by the individual side bands.

### B. Accuracy of Small-Signal Modelling

In the radial system of Fig. 1 when the upstream supply voltage is sinusoidally amplitude modulated, the downstream voltage would contain additional frequency components at $f_b \pm nf_m$ ($n \neq 1$) caused by multiple armature reaction of the motor as discussed in [6] and hence the flicker transfer behavior may not only be governed by the two side bands of the sinusoidally amplitude modulated voltage waveform. In the small-signal model of the system presented in Section III, the additional frequency components $f_b \pm nf_m$ are not accounted for as a part of the linearization process. Hence, it is required to investigate the accuracy of the use of the small-signal model in establishing the flicker transfer coefficient.

The flicker transfer coefficients established for the 2250 hp machine using the small and large-signal models are compared for the radial system (with a system impedance of 3%) in Fig. 13. The error involved in the evaluation of the flicker transfer coefficient using the small-signal model is established using the absolute difference between the $T_{Pst}$ values determined using the small and large-signal models expressed as a percentage of the $T_{Pst}$ determined using the large-signal model. Fig. 14 illustrates the variation of the error with modulation frequency where it can be noted that the maximum error is around 0.5% which occurs at very low modulation frequency $f_m = 0.01$ Hz. This simply means that the additional frequency components ($f_b \pm nf_m$) that have been neglected in the small-signal modelling do not have a significant impact on the flicker transfer coefficient. Hence, it can be concluded that the small-signal model is accurate enough to investigate the response of the induction motors in relation to flicker transfer and attenuation.

## VI. Conclusion

As a continuation of the work presented in [6], investigations have been carried out to examine the contribution of induction motor loads to flicker attenuation in radial power systems. A small-signal model was used to represent the dynamic nature of an induction motor and to establish the transfer coefficients of the voltage perturbations which exist as side bands of the amplitude modulated supply.

The magnitude of the effective sub or supersynchronous impedance $(Z'_{\text{motor}})$ of the 2250 hp induction motor was found to be relatively small compared to its steady state value for most of the voltage side band frequencies. The angle of $Z'_{\text{motor}}$ was found to vary over a wide range exhibiting inductive or capacitive behavior affecting voltage side band attenuation or magnification. The variation of the effective impedance can be attributed to the way the motor responds to each side band frequency. Consequently, the attenuation of voltage side bands and that of flicker was found to be dependent on the frequency of voltage side band $(f_b \pm f_m)$, and hence on the modulation frequency $(f_m)$. As the modulation frequency increases, the attenuation of side bands and hence that of flicker was seen to increase except at very low modulation frequencies.

The transfer coefficient of a voltage side band ($T_{LSB}$ or $T_{USB}$) depends on the size of the induction motor. Amongst the three machines examined, larger machines have shown similar flicker attenuation characteristics compared to the smaller machine. Attenuation of side bands depends on the magnitude and the angle of the system impedance $(Z_s)$. Large inductive system impedances would result in smaller transfer coefficient for the side bands.

This paper presented the results of detailed theoretical investigations which further support that induction motors do assist in attenuating flicker at downstream bus bars.

## ACKNOWLEDGMENT

The authors would like to thank Dr. D. Geddey of TransGrid and TransGrid, New South Wales, Australia, for financially supporting the project.

## REFERENCES

[1] E. De Jaeger, G. Borloo, and W. Vancoetsem, "Flicker transfer coefficients from HV to MV and LV systems," in *Proc. 14th Int. Conf. Electricity Distribution, (CIRED97)*, Birmingham, U.K., Jun. 1997, pp. 101–102, Session 2.

[2] S. M. K. Tennakoon, L. Perera, D. Robinson, and S. Perera, "Flicker transfer in radial power systems," presented at the Proc. Australasian Universities Power Engineering Conf. (AUPEC), Brisbane, Australia, Sep. 2004, Paper 190, unpublished.

[3] M. C. Simöes and S. M. Deckmann, "Flicker propagation and attenuation," in *Proc. 10th Int. Conf. Harmonics and Quality of Power*, Oct. 2002, vol. 2, pp. 644–648.

[4] H. Renner and M. Sakulin, "Flicker propagation in meshed high voltage networks," in *Proc. 9th Int. Conf. Harmonics and Quality of Power*, Oct. 2000, vol. 3, pp. 1023–1028.

[5] S. Perera, D. Robinson, S. Elphick, D. Geddey, N. Browne, V. Smith, and V. Gosbell, "Synchronised flicker measurement for flicker transfer evaluation in power systems," *IEEE Trans. Power Del.*, vol. 21, no. 3, pp. 1477–1482, Jul. 2006.

[6] S. Tennakoon, S. Perera, and D. Robinson, "Flicker attenuation—Part I: Response of three phase induction motors to regular voltage fluctuations," *IEEE Trans. Power Del.*, vol. 23, no. 2, pp. 1207–1214, Apr. 2008.

[7] *Electromagnetic Compatibility (EMC)—Limits—Assessment of Emission Limits for Fluctuating Loads in MV and HV Power Systems*, IEC/TR 61000-3-7, 1996, Ed. 1.0.

[8] *Electromagnetic Compatibility (EMC)—Limits—Assessment of Emission Limits for Fluctuating Loads in MV and HV Power Systems (IEC 61000-3-7:1996, MOD)*, AS/NZS 61000.3.7:2001, *Standards Australia*.

[9] P. C. Krause, O. Wasynczuk, and S. D. Sudhoff, *Analysis of Electric Machinery*. New York: McGraw-Hill, 1986, pp. 189–203.

**S. Tennakoon** (S'06) received the B.Sc. (Hons.) degree in electrical power engineering from the University of Moratuwa, Sri Lanka. Currently, she is pursuing the Ph.D. degree at the University of Wollongong, Wollongong, Australia.

She is a recipient of an International Postgraduate Research Scholarship (IPRS) from the University of Wollongong. Her research interests are in power quality and electrical machine modelling.

**S. Perera** (M'95) received the B.Sc. degree in electrical power engineering from the University of Moratuwa, Sri Lanka, the M.Eng.Sc. degree from the University of New South Wales, Australia, and the Ph.D. degree from the University of Wollongong, Wollongong, Australia.

He has been a Lecturer at the University of Moratuwa, Sri Lanka. Currently, he is an Associate Professor with the University of Wollongong and is the Technical Director of the Integral Energy Power Quality and Reliability Centre at the University of Wollongong, Australia.

**D. Robinson** received the B.E. (Hons.) degree and the Ph.D. degree in harmonics management from the University of Wollongong, NSW, Australia.

He was previously with BHP Steel and the University of Wollongong. Currently, he is with Beca Pty Ltd, Wollongong, Australia.